EFFECT OF INTERNAL HYDROGEN ON THE MIXED-MODE I/III FRACTURE TOUGHNESS OF A FERRITIC/MARTENSITIC STAINLESS STEEL - H. Li (Associated Western Universities—Northwest Division), R. H. Jones (Pacific Northwest Laboratory[a]), J. P. Hirth (Washington State University) and D. S. Gelles (Pacific Northwest Laboratory[a]).

OBJECTIVE

To investigate the effect of hydrogen on mode I and mixed mode I/III fracture toughness at room temperature for a low activation ferritic/martensitic stainless steel (F82-H).

SUMMARY

The effects of H on the mixed-mode I/III critical *J*-integrals (J_{TQ}) and tearing moduli (dJ/da) were examined for a ferritic/martensitic stainless steel at ambient temperature. A H content of 4 ppm(wt) was attained after charging in a H_2 gas chamber (138 MPa) at 300°C for 2 weeks. Results showed that H decreased J_{TQ} and dJ/da values compared to steel tested without H. However, the presence of H did not change the dependence of J_{TQ} and dJ/da values on crack angle. Both J_{IQ} and dJ_I/da exhibited the highest relative values. The minimum values of both J_{TQ} and dJ/da occurred at a crack angle between 35 and 55° [$P_{III}/(P_{III} + P_I) = 0.4$ and 0.6]. A mechanism of the combined effect of H and mixed-mode on J_{TQ} and dJ/da is discussed.

INTRODUCTION

Traditionally, mode I fracture has been used to study elastic-plastic fracture mechanics. However, in recent years, mixed-mode fracture has become a focus of many studies, in particular for the mixed-mode I/III case [1-9]. In tough materials [such as a high-purity rotor steel (HPRS) [5,6], which fail primarily by a microvoid nucleation and growth mechanism], the presence of a mode III loading component lowers the J_{TQ} values considerably from their mode I values. The J_{TQ} values pass through a minimum at a position between mode I and mode III on a plot of J_{TQ} vs crack inclination angle. More generally, materials can be divided into three categories according to their process zone size as presented by J_{TQ}/σ_Y and the ratio of J_{TQ} (at crack angle of 45°) to J_{IQ}, as shown in Fig. 1 [10]. The materials in Region I are brittle and sensitive to mode I loading and, consequently, mode I fracture toughness is the lowest as compared with mixed-mode I/III fracture toughness. Therefore, for such materials, mode I fracture toughness is properly used for design. Those materials in Region II are tough and sensitive to mixed-mode I/III loading, mode I fracture toughness is no longer the largest, and the minimum mixed-mode J_{TQ} is recommended as a design criterion. For the materials in Region III, mode I and mixed-mode fracture toughness are similar and the mode I value can be used for design with small uncertainty. Our results [11,12] on the fracture toughness of a F-82H steel showed that the steel is a tough material which falls in Region II in Fig. 1. The presence of a mode III stress component lowers its fracture toughness significantly. However, the minimum upper shelf fracture toughness is still higher than the J_{IQ} values for most tough materials that have been tested.

Structural materials in fusion energy systems will be exposed to hydrogen (H) from the plasma and (n, σ) reactions. For a tough rotor steel, the introduction of H was found to decrease the overall mixed-mode I/III fracture toughness [6,13]. Hence, an investigation of the combined effects of mixed-mode loading and H on the fracture toughness of F-82H steel was undertaken to determine its suitability for fusion power reactor applications. The other purpose was to further study the mechanism by which H affects the mixed-mode I/III fracture toughness.

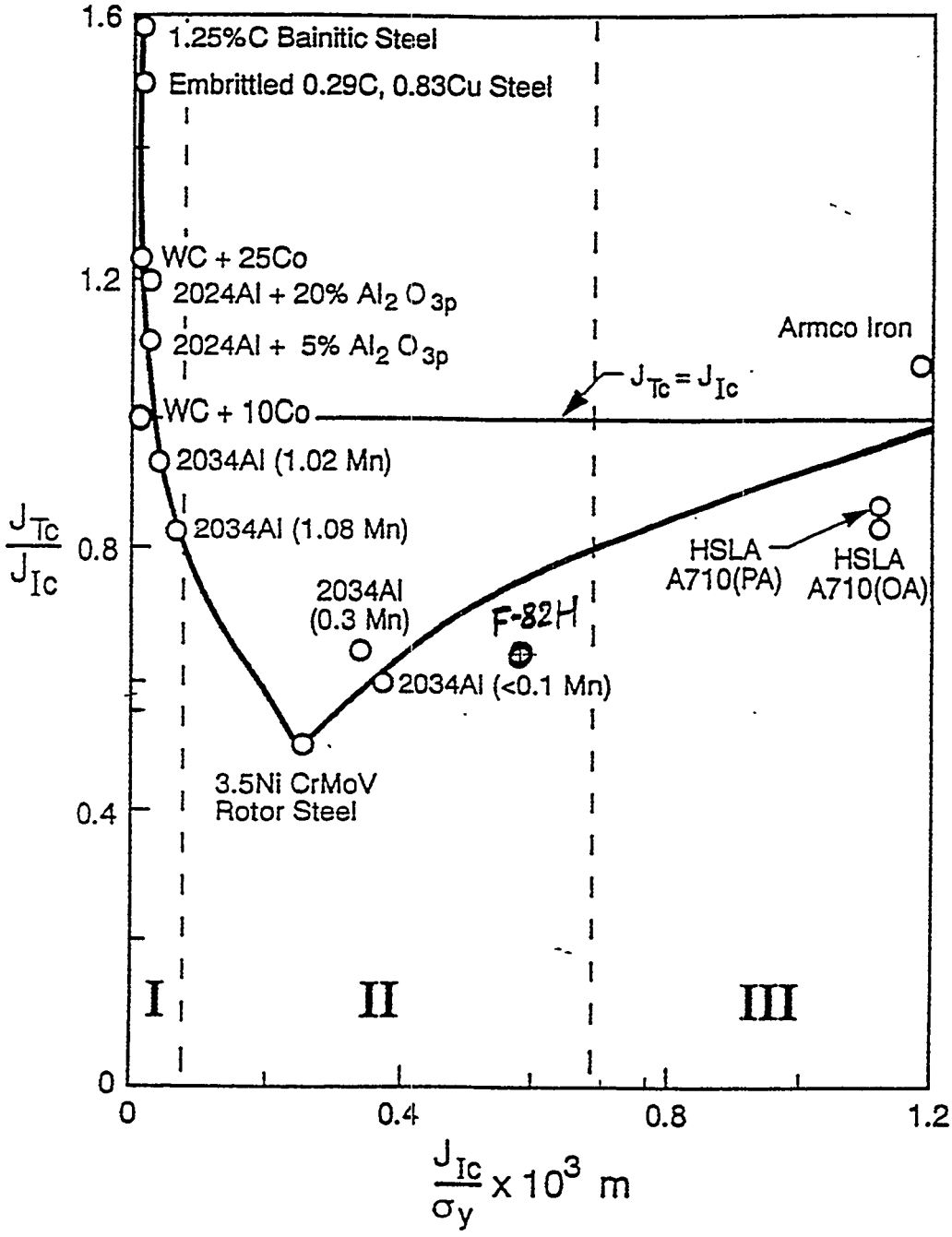

Fig. 1. J_{TC}/J_{IC} versus J_{Ic}/σ_y for different materials; where J_{TC} is the mixed-mode I/III J-integral at σ_{iii}/σ_i = 1, and σ_y is yield strength. The materials in Region I, II, and III are low toughness, tough, and ductile/tough materials, respectively.

MATERIAL AND EXPERIMENTAL METHODS

1. Material and Hydrogen-Charging

The F-82H steel plate used in this study was supplied by the Nippon Kokan Steel Company (NKK) in Japan. The chemical composition of the plate (as provided by NKK) is (by wt%): 0.096C-7.71Cr-2.1W-0.18V-0.04Ta-0.003P-0.003S. Specimens used in this study were cut in the T-L orientation as specified in ASTM E399-90 and were given a heat-treatment of 1000°C/20h/air cooling (AC), 1100°C/7min/AC, and 700°C/2h/AC. The resulting microstructure was tempered martensite. The mean intercept grain size was 25 μm. The heat-treatment resulted in a yield strength (σ_y) of 648 MPa, an ultimate tensile strength (σ_{uts}) of 735 MPa, an elongation of 16.7%, and a reduction in area of 70%.

H-charging was performed at Sandia National Laboratories, Livermore, CA. The specimens were charged with H at a H_2 gas pressure of 138 MPa at 300°C for two weeks, which resulted in a H content of 4 ppm(wt). H contents were measured with the inert gas fusion technique. A Cu coating was applied immediately after H-charging. The specimens with Cu coating were stored at -60°C. Before *J*-integral testing commenced, a specimen was warmed up to 24°C. *J* testing took about 60 minutes. H loss during *J* testing was minimized because of a low H diffusivity in ferritic/martensitic stainless steel at 24°C [14] and the added barrier of the Cu coating.

2. Experimental Methods

The geometry of the modified compact-tension specimens used for mixed-mode I/III testing is schematically shown in Fig. 2. The magnitude of the mode III loading components (P_{iii}) can be varied by changing the crack slant angle Φ since $P_{iii} = P_{appl} \sin \Phi$, where P_{appl} is the applied load. An angle of 0° represents mode I loading and the geometry of a 0° specimen becomes the standard compact-tension specimen as specified in ASTM standard E813-89. As Φ increases, the contribution of the mode III loading components increases. The crack-inclination angles used in this study were 0, 15, 25, 35, 45, and 55°. Side grooves of 20% reduction of total thickness were incorporated in all specimens. These side grooves increase the stress triaxiality at the edges of a growing crack and serve to constrain the advancing crack in the original crack plane. The calculation of the *J*-integrals in mixed-mode I/III requires a measurement of both vertical displacement (δ_v) and horizontal displacement (δ_h) of the load points. A pair of knife edges was secured to the front face of a specimen. A standard crack opening distance clip gage was positioned on the knife edges. The load-line δ_v values were calculated from the front face δ_v values with the method proposed by Saxena and Hudak, Jr. [15]. We found that δ_h increased with δ_v in a linear manner [1,3]. Hence, δ_h values were calculated approximately from the relation $\delta_h = \alpha\delta_v$, where $\alpha = \delta_{hmax}/\delta_{vmax}$.

An electric discharge machine (EDM) was used to make thin cuts with a small radius (radius = 0.051 mm) and approximately 1.3 mm long. The cuts were used as a substitute for a fatigue pre-crack (FPC) because an FPC tends to grow out of the original crack plane in mixed-mode specimens. The EDM cuts were made after final heat-treatment. The single-specimen technique was used in this study, which allows a *J-R* curve (*J* vs crack extension Δa) to be generated with one specimen. During testing, the specimen was frequently and partially unloaded, and the partial unloading compliances were used to calculate the corresponding crack lengths following the procedure described in ASTM E813-89 and by Li et al [15]. *J* values matching those crack lengths were also calculated by means of Eq. (1) in the next section. At least 20 pairs of *J*-Δa data were used to construct a *J-R* curve.

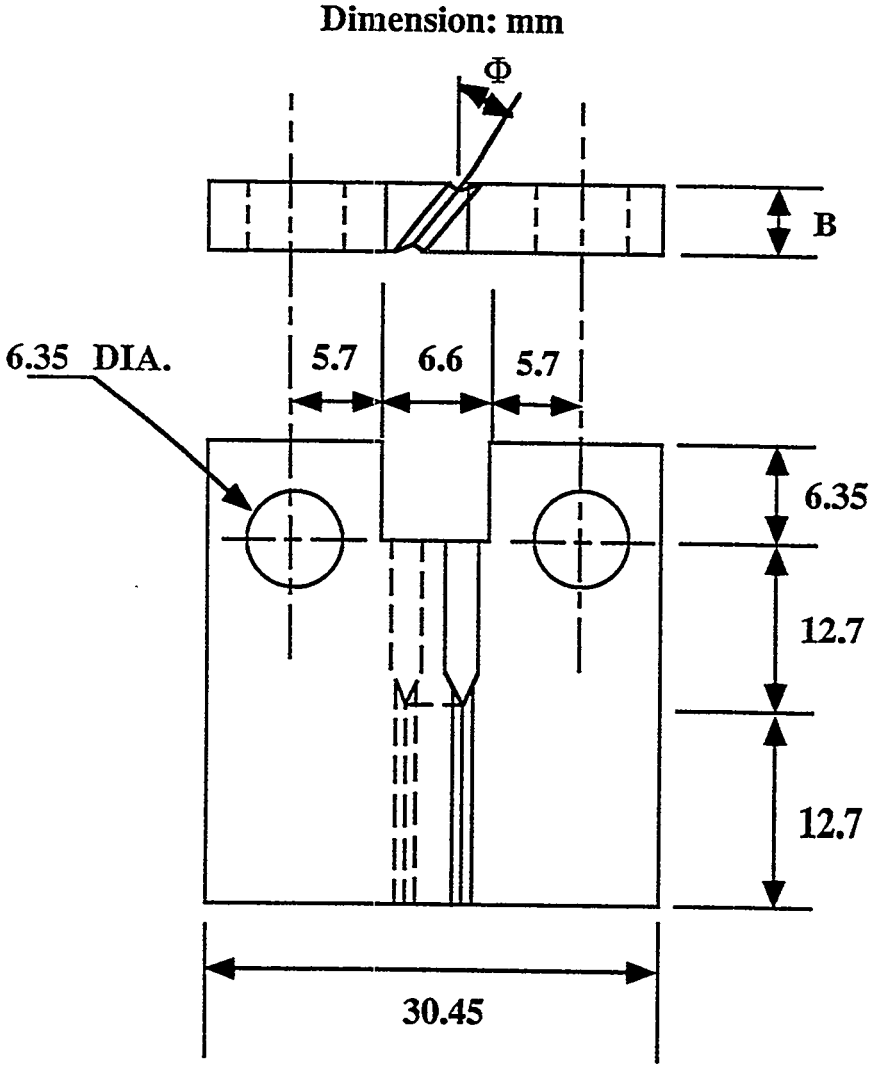

Fig. 2. The geometry of a modified compact tension specimen.

All of the fracture surfaces were examined by means of a scanning electron microscope (SEM) with an attached energy-dispersive X-ray spectroscope. A stereo microscopy technique [16] was used to study asperities on fracture surfaces.

DATA ANALYSIS

The mode I J_I and mixed mode I/III J_T were calculated from the area under the load vs load-line-displacement curve by means of Eq. (1) [17]:

$$J = \frac{2}{B_{net}\, b_o} \int_0^{\delta_v} P\, d\delta_v \qquad (1)$$

where

B_{net} = 0.8B/cosΦ (the net crack front width excluding the 10% side grooves on each side)
B = the overall specimen thickness
Φ = the crack-inclination angle
b_o = W - a_o
W = the specimen width
a_o = the initial physical crack length.

To construct *J-R* curves and determine critical *J* values (J_{IQ} and J_{TQ}), the ASTM E813-89 procedure was used. The subscript "Q" was used because F82-H steel was so tough that the specimen thickness did not meet the plane strain requirement. Since there is no standard for constructing a mixed-mode I/III blunting line, the analogy to the case of pure mode I was used. The slope of the blunting line for mixed mode I/III was calculated from Eq. (2):

$$m_{i/iii} = \frac{m_i \cos\Phi + m_{iii} \sin\Phi}{\sin\Phi + \cos\Phi} \qquad (2)$$

where $m_i = (\sigma_y + \sigma_{uts})$ and $m_{iii} = (\sigma_y + \sigma_{uts})/2$, which are the blunting line slopes for pure mode I and mode III loading, respectively. When Φ equals 0 or 90°, $m_{i/iii}$ is equal to m_i or m_{iii}, respectively. A best-fit straight line was also constructed from the *J*-Δ*a* data between the upper and lower exclusion lines, and the slope of the straight line was taken as the unnormalized tearing modulus (dJ_I/da or dJ_T/da) for each specimen. The critical mode I and mode III *J* components (J_{ic} and J_{iiic}) in mixed-mode specimens also could be calculated in terms of the corresponding resolved loads and displacements. The methods of calculation of the resolved mode I and mode III load components (P_i and P_{iii}) and displacement components (δ_i and δ_{iii}), and the determinations of J_{ic} and J_{iiic} have been reported in detail in Refs. 6, 7, and 12.

RESULTS

1. The Critical *J* Values and the Tearing Moduli (*dJ/da*)

The effect of H on J_{TQ} is shown in Fig. 3. In the limit of Φ = 0°, J_{TQ} is equal to J_{IQ}; for 0< Φ <90°, J_{TQ} represents the total critical *J* value under mixed-mode loading. The J_{TQ} values for specimens without H are also included for comparison. From Fig. 3, one can see that the introduction of H into the F-82H steel decreases its overall fracture toughness considerably, to a degree which is independent of crack angle. However, the presence of H did not change the trend of the *J*-[$P_{iii}/(P_{iii} + P_i)$] curve; J_{IQ} is still the highest *J* value. As [$P_{iii}/(P_{iii} + P_i)$] increases, J_{TQ} decreases until it reaches a minimum at a [$P_{iii}/(P_{iii} + P_i)$] ratio between 0.4 and 0.6, corresponding to a crack angle range of 35 to 55°. The change of J_{TQ} with [$P_{iii}/(P_{iii} + P_i)$] is similar to that for a steel without H, and follows a second-order polynomial function. The effect of H on J_{TQ} of the F-82H steel is similar to that for another tough steel, HPRS [6,13], in which the addition of H also lowered the overall J_{TQ}. However, the minimum J_{TQ} for H-charged F-82H steel is around 100 kJ/m^2, higher than the value of 64 kJ/m^2 reported for the HPRS [6,13].

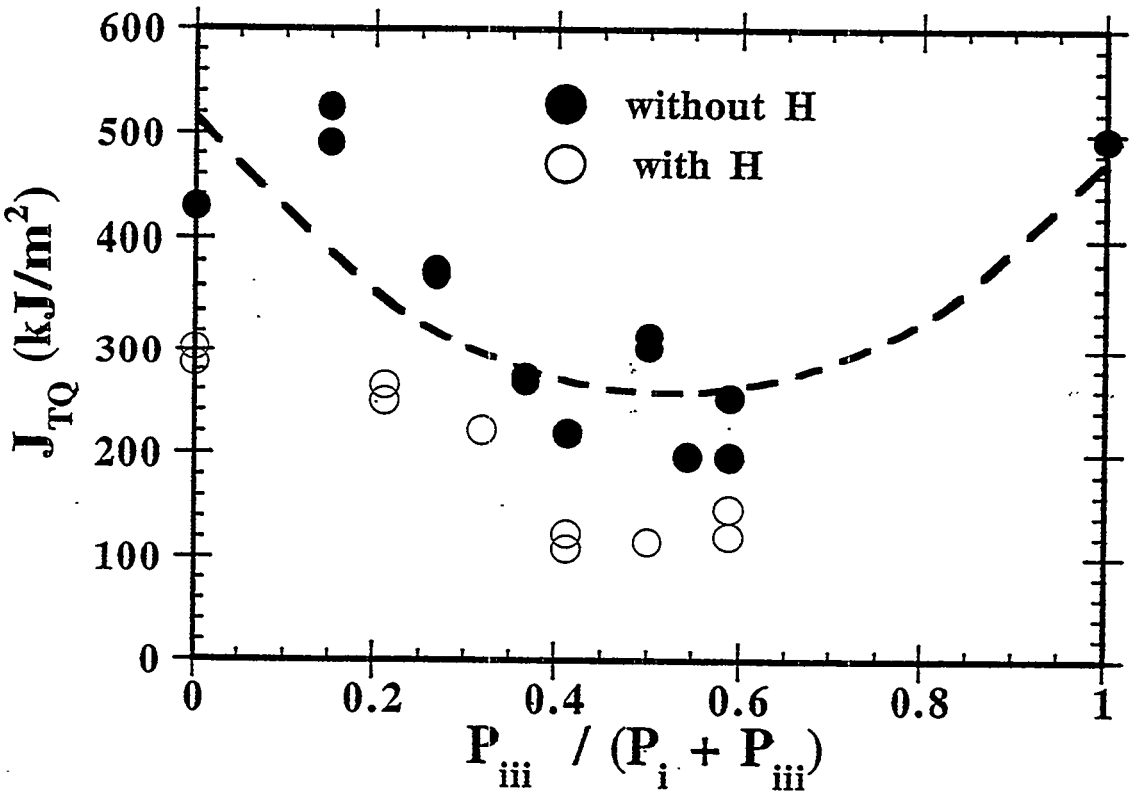

Fig. 3 The dependence of J_{TQ} on mode III loading component.

The introduction of H also reduced the resistance to crack growth, i.e. lowered the overall mixed-mode *dJ/da* relative to the steel without H. The unnormalized *dJ/da* corresponding to different $[P_{iii}/(P_{iii} + P_i)]$ values are shown in Fig. 4. From Fig. 4, one can see that H does not change the dependence of *dJ/da* on $[P_{iii}/(P_{iii} + P_i)]$. The variation of *dJ/da* with $[P_{iii}/(P_{iii} + P_i)]$ is also found to obey a second-order polynomial, similar to the curve without H.

2. Fractography

The crack fronts of all specimens remained in their initial orientation during *J* testing. Investigation of fracture surfaces with SEM showed that internal H in the F-82H steel did not induce intergranular or cleavage facets. All of the specimens exhibited a microvoid coalescence type of fracture, as shown in Fig. 5. Most of the larger voids initiated from sulfide particles and the spacing of the finer voids is consistent with nucleation at tempered carbide particles. But, H appeared to affect the processes of void initiation and coalescence. Fig. 6 shows two pairs of low magnification (about 4 X) fracture surfaces, mode I specimens ($\Phi = 0°$) and mixed-mode I/III specimens ($\Phi = 35°$), respectively. Fig. 6 indicates that a specimen with H has less thickness reduction (%TR) at the crack tip and critical crack tip opening (COD)

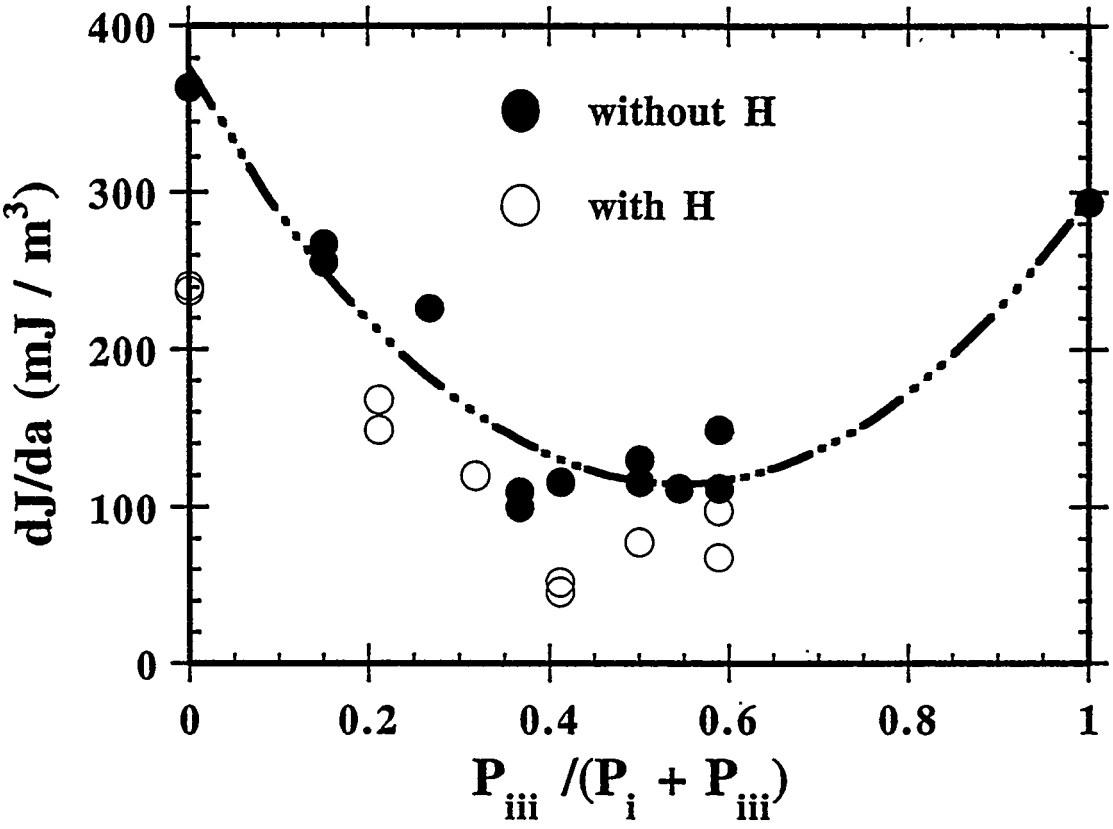

Fig. 4. The dependence of *dJ /da* on mode III loading component.

than those without H. The data of the %TR and COD values for these specimens are listed in Table 1 along with the corresponding J_{TQ} values. Evidently, the effect of H on J_{TQ}, COD and the %TR values of the F-82H steel is consistent in that the cases with lower J_{TQ} values with H present corresponded to the cases of little lateral necking and crack tip plastic deformation prior to final fracture. Furthermore, H decreased the roughness of fracture surfaces in all specimens (Fig. 6). While the difference on the 0° specimens is not as evident as that on the 35° specimens at low magnification, it is manifested at higher magnification (Figs. 7a and 7b). Overall, the crack has very high tortuosity. Stereo pair SEM views of regions such as that in Fig. 7a show that reentrant regions on one surface match salient features on the other and vice-versa, with slopes of up to about ±45°. Thus, at the coarsest size scale, the crack is locally a mixed-mode I-II-III crack with large roughness. At the next level, the larger dimples reflect voids at the 3-10 μm scale and usually contain sulfide particles. Those can be seen in Fig. 8a and 8b. At the finest scale, there are more fine voids, 0.5-1 μm, in the presence of H and these voids tend to be flatter. The smaller microvoid size in the H-charged specimens indicated that H facilitated void initiation and coalescence. The overall flatter and more well defined tear ridges in the H-charged case showed that H avored cracking along the trajectories of intense shear flow, resulting in lower J_{TQ} and *dJ/da* values.

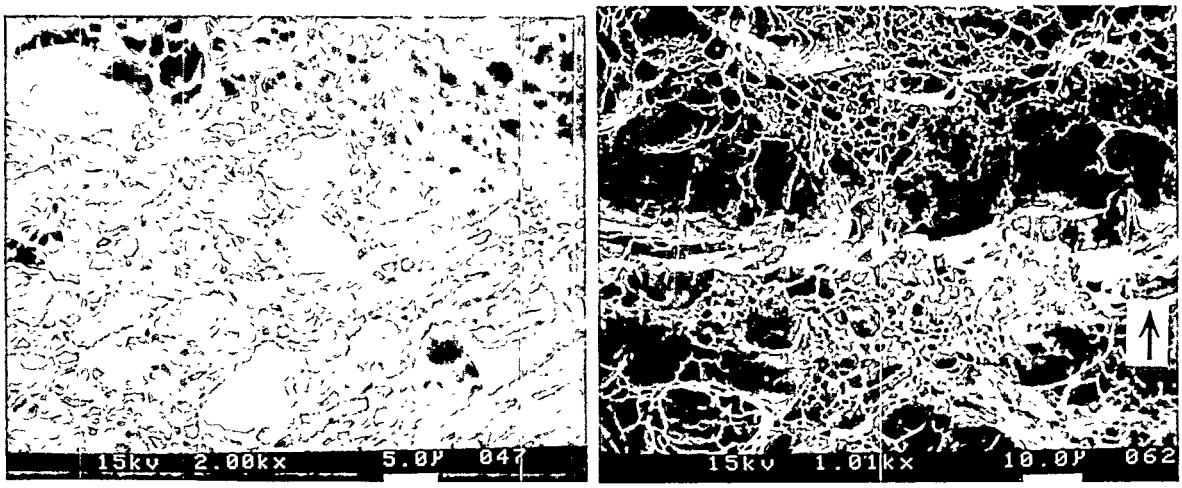

(a) (b)

Fig. 5. SEM fractographs showing the microvoid coalescence nature fracture surfaces. (a) Mode I specimen; (b) 35° specimen. The arrow indicates shear direction.

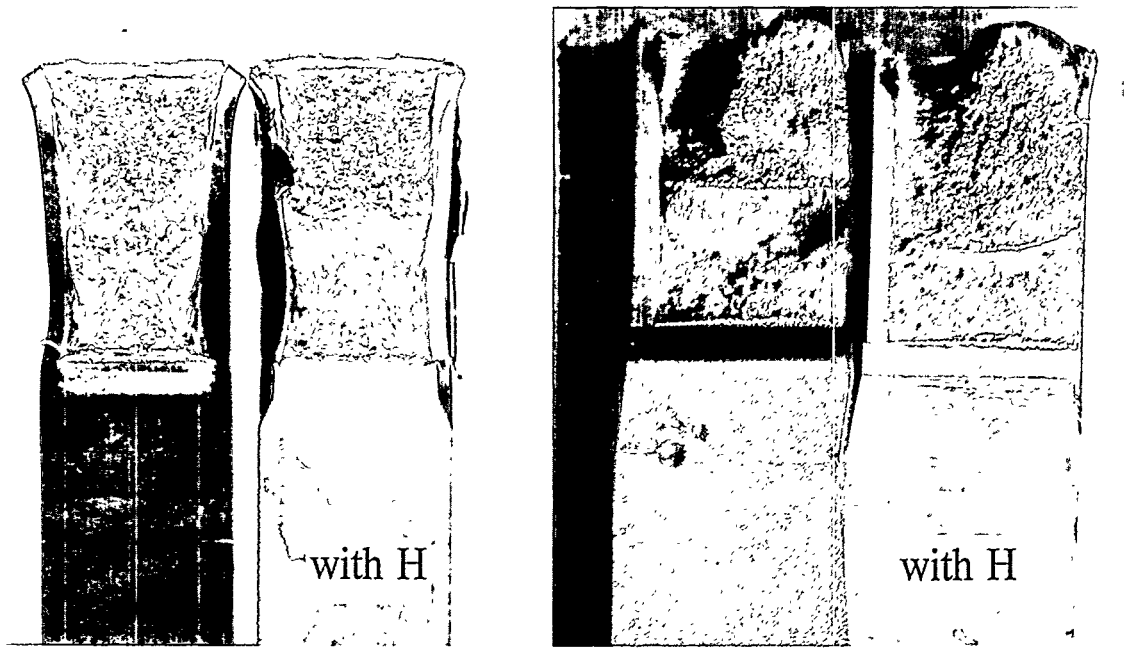

(a) (b)

Fig. 6. Optical microscope photos showing the effects of H on thickness reduction at the crack tips and roughness of fracture surfaces. a. Mode I specimen; b. 35° specimen.

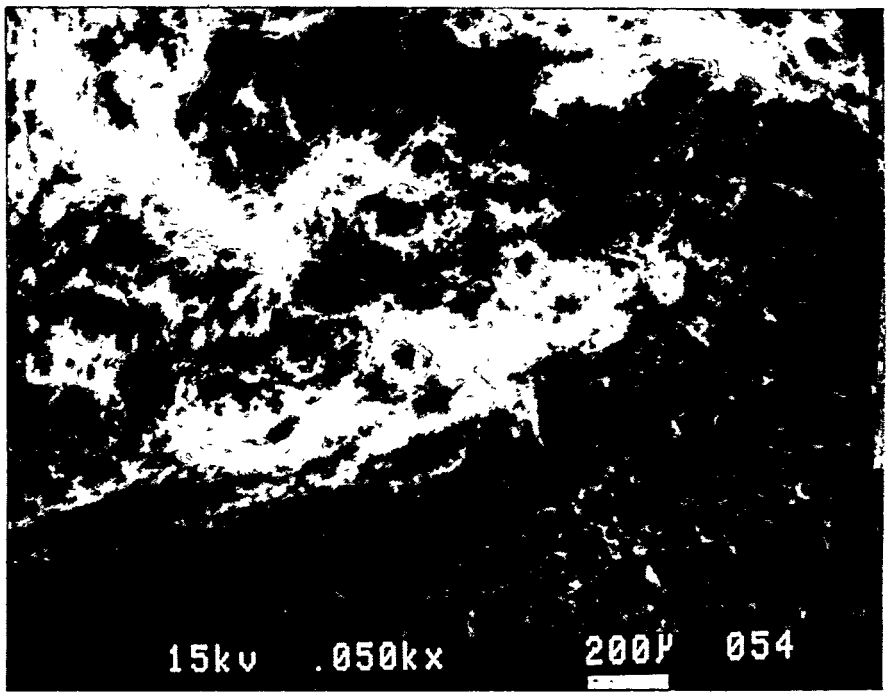

(a)

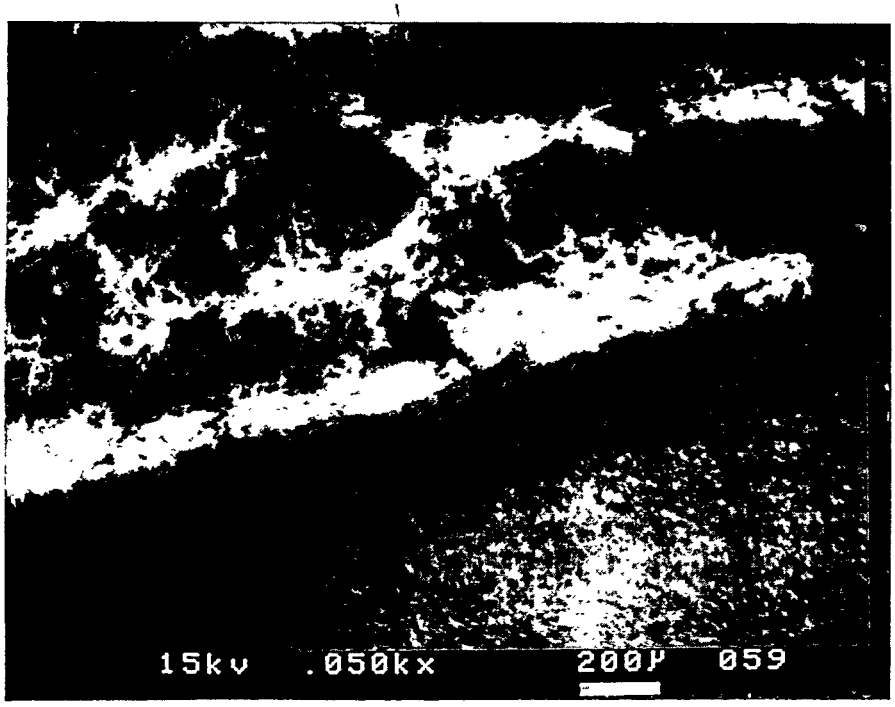

(b)

Fig. 7. SEM fractographs of mode I specimens showing the effect of H on void size. a. Without H; b. with H.

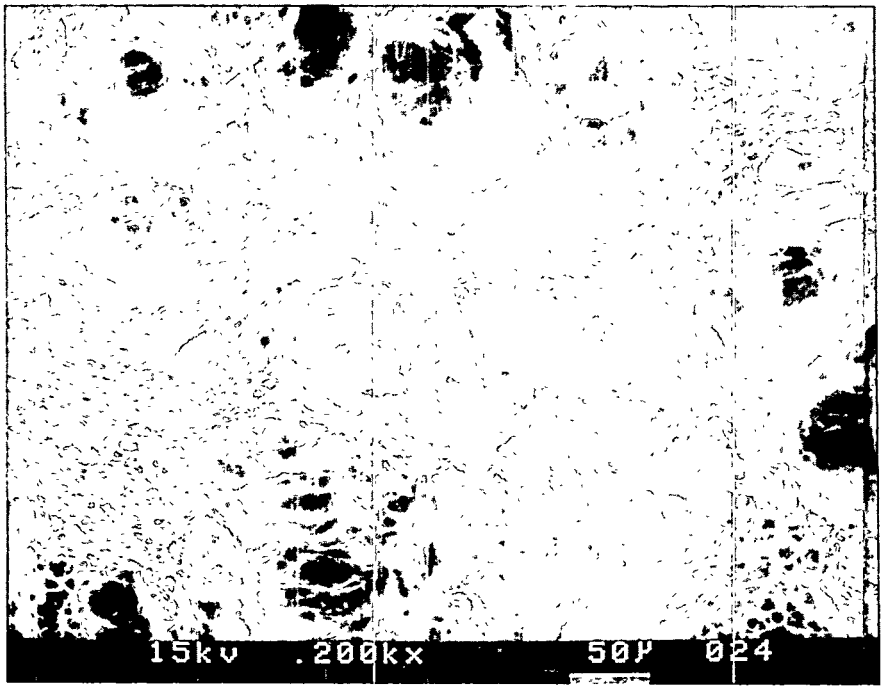

(a)

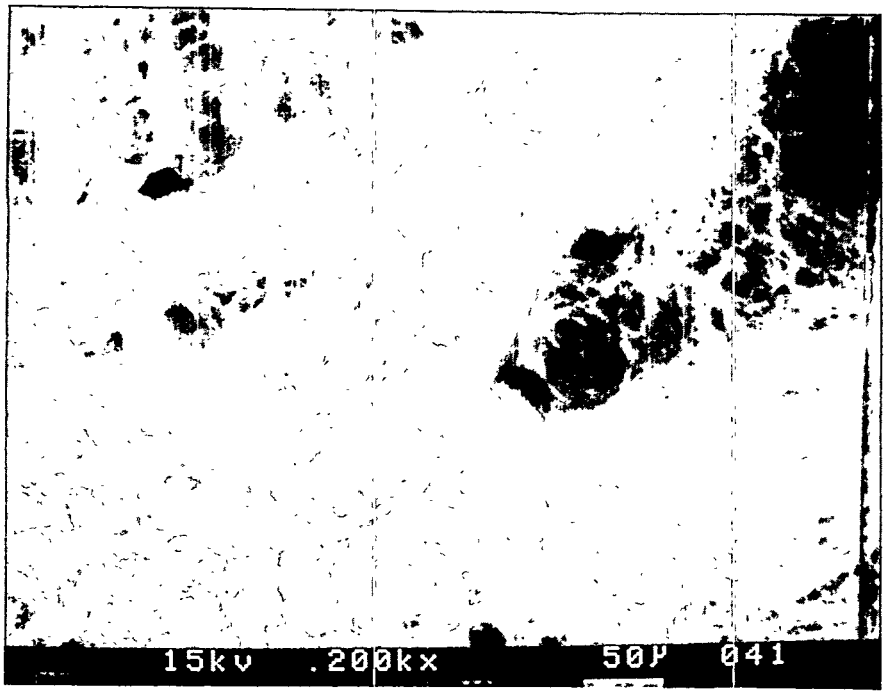

(b)

Fig. 8. SEM micrographs of mode I specimens at higher magnification showing the effect of H on void size. a. Without H; b. with H.

Table 1. Effect of H on J_{TQ}, thickness reduction (%TR) & COD (δ)

Crack angle	0°		35°	
	with H	no H	with H	no H
J_{TQ} (kJ/m^2)	303	429	110	219
%TR	11	16	≈ 0	≈ 3
δ_{meas}* (mm)	.37	.58	.24	.36
δ_{cal} (mm)	.41	.60	.16	.31

* Subscript "meas" and "cal" mean measured and calculated values.

DISCUSSION

The addition of a mode III loading component to mode I loading has been found to increase, decrease, or have little or no effect on the J_{TQ}, depending on the toughness of the materials. For brittle materials, such as glass [18], 0.29C-0.83Cu, steel and 1.25C bainitic steels [4,8-10], in which fracture was controlled by tensile stress and the local crack-opening displacements, the addition of mode III loading components had little or no effect on the values of J_{ic}, but tended to increase J_{TQ}. For tough steels, such as HPRS [6], which failed primarily by microvoid coalecense, the presence of shear strain in the crack plane associated with mode III loading produced incompatibility stresses at the particle interfaces in the trajectory of the crack, causing decohesion or particle fracture (shear damage). This process led to enhanced void formation that limited the mode I plastic flow field and caused premature separation of voids by the mode I normal stress. Accordingly, tough materials exhibited a lower fracture toughness for a mixed-mode crack than for a mode I crack. For those materials with intermediate toughness, such as AISI 1090 steel, the addition of a mode III loading component decreased J_{ic} moderately, and had little effect on J_{TQ}.

As seen from Fig. 3, the F-82H steel is very tough and very sensitive to incompatibility stresses at particle interfaces caused by the mode III loading component. Under mixed-mode loading, J_{TQ} decreased as the mode III load component increased, reaching a minimum at a crack angle between 40 and 50°.

The issue remains regarding the mechanism for the degrading effect of H in the F82-H steel, in which H degrades the properties but leaves the ductile fracture mechanism unchanged. A variety of studies of such steels in plane strain tension [17-28] have shown that H promotes the onset of plastic instability in the form of shear localization. In relatively pure, single phase materials, this may be the consequence of a lowered flow stress for dislocation glide [29-31] or a tendency for increased coplanarity of slip [32]. In multiphase engineering materials, the effect instead is associated with localized damage in the form of enhanced void formation by particle decohesion and cracking [31-36] and of enhanced void growth and agglomeration [33-35]. Voids also enhance shear localization [36-38]. Thus, the H enhances void formation, which enhances shear localization, which in turn enhances further void formation because of incompatibility effects. This autocatalytic phenomenon leads to failure at lower strains in the presence of H.

Fractographic analysis indicates that H plays a similar role in reducing J_{TQ} in H-charged F-82H steel. The out-plane shear strain induced by a mode III loading component caused shear damage in the form of void initiation at sulfides and carbides. The presence of H further enhances void formation, growth and

agglomeration, consistent with the tensile test results [31-38] and thereby enhances the degradation of toughness. Hence, the combined effect of H and mode III shear stress made crack initiation and growth easier, resulting in lower J_{TQ} and dJ/da in H-charged F-82H steel at all crack angles.

CONCLUSION

The presence of H reduced both J_{TQ} and dJ/da for a ferritic/martensitic stainless steel, independent of crack slant angles. However, H did not change the dependence of J_{TQ} and dJ/da on crack angles. Both J_{IQ} and dJ_I/da exhibited the highest values, the minimum J_{TQ} and dJ/da were attained at a crack angle between 35 and 55°, where the ratio of $P_{iii}/(P_{iii} + P_i)$ is between 0.4 and 0.6. However, the minimum J_{TQ} remained high, at about 100 kJ/m^2.

ACKNOWLEDGEMENTS

We are grateful to Dr. N. R. Moody of Sandia National Laboratories, Livermore, CA for H-charging. The assistance of Mr. J. L. Humason at Pacific Northwest Laboratory in developing the test methods is gratefully acknowledged. This research was supported by the Office of Fusion Energy of the U. S. Department of Energy under Contract DE-AC06-76RLO 1830 with Battelle Memorial Institute.

REFERENCES

1. M. T. Miglin, I.-H. Lin, J. P. Hirth, and A. R. Rosenfield, in Fracture Mechanics: 14th Symp. — Vol. II: Testing and Applications, ASTM STP 791, J. C. Lewis and G. Sines, Eds., ASTM, Philadelphia, 1983, pp. II-353-II-369.

2. M. T. Miglin, J. P. Hirth, and A. R. Rosenfield, Res. Mech., 11 (1984), pp. 85-95.

3. J. G. Schroth, J. P. Hirth, R. G. Hoagland, and A. R. Rosenfield, Met. Trans. A, 18A (1987), pp. 1061-1072.

4. M. Manoharan, J. P. Hirth, and A. R. Rosenfield, J. of Test. and Eval., 18 (1990), No.2, pp. 106-114.

5. S. Raghavachary, A. R. Rosenfield, and J. P. Hirth, Met. Trans. A, 21A (1990), pp. 2539-45.

6. J. A. Gordon, J. P. Hirth, A. M. Kumar, and N. R. Moody, Jr., Met. Trans. A, 23A (1991), pp. 1013-1020.

7. M. Manoharan, S. Raghavachary, J. P. Hirth, and A. R. Rosenfield, J. Eng. Mater. Technol., 111 (1989), pp. 440-442.

8. A. M. Kumar and J. P. Hirth, Scripta Metall. Mater., 25 (1991), pp. 985-90.

9. M. Manoharan, J. P. Hirth, and A. R. Rosenfield, Scripta Metall. Mater., 23 (1989), pp. 763-766 and pp. 1647-1648.

10. S. V. Kamat and J. P. Hirth, Scripta Metall. Mater., 30 (1994), pp. 145-48.

11. Huaxin Li, R. H. Jones, J. P. Hirth, and D. S. Gelles, J. of Nuclear Materials, 1994, in press.

12. Huaxin Li, R. H. Jones, J. P. Hirth, and D. S. Gelles, Metall. and Mater. Trans. A, 1994, submitted.

13. A. M. Kumar, N. R. Moody, Jr., J. P. Hirth, and J. A. Gordon, Met. Trans. A, 24A (1993), pp. 1450-1451.

14. J. Xu, X. Z. Yuan, X. K. Sun and B. M. Wei, Scripta Metall. Mater., 29 (1993), pp. 925-30.

15. Ashok Saxena and S. J. Hudak, Jr, Int. J. Fract., 14 (1978), pp. 453-468.

16. D. S. Gelles and F. H. Huang, in Alloy Development for Irradiation Performance, Semiannual Progress Report, DOE/ER-0045/8, Oak Ridge National Lab., Oak Ridge, TN (March 31, 1982), pp. 442-459.

17. J. R. Rice, P. C. Paris, and J. G. Merkle, in ASTM STP 536, ASTM, Philadelphia, 1973, pp. 231-235.

18. A. R. Rosenfield and W. H. Duckworth, Int. J. Fract., 32, (1987), p. R59.

19. A. W. Thompson and I. M. Bernstein, in Proc. Hydrogen in Metal Congress, Paris, France, Pergamon Press, Oxford, 1977, vol. 3, pp. 1-8.

20. T. D. Lee, T. Goldenberg, and J. P. Hirth, Metall. Trans. A, 10A (1979), pp. 199-208.

21. T. D. Lee, T. Goldenberg, and J. P. Hirth, Metall. Trans. A, 10A (1979), pp. 439-48.

22. O. A. Onyewuenyi and J. P. Hirth, Metall. Trans. A, 14A (1983), pp. 259-69.

23. S. C. Chang and J. P. Hirth, Metall. Trans. A, 17A (1986), pp. 1485-7.

24. A. Chatterjee, R. G. Hoagland, and J. P. Hirth, Mater. Sci. and Engin., A142 (1991), pp. 235-43.

25. I. G. Park and A. W. Thompson, Metall. Trans. A, 21A (1990), pp. 465-77.

26. I. G. Park and A. W. Thompson, Metall. Trans. A, 22A (1991), pp. 1615-26.

27. C. Hwang and I. M. Berstein, Acta Metall., 34 (1986), pp. 1001-10, pp. 1011-20.

28. T. D. Lee, I. M. Bernstein, and S. Mahajan, Acta Metall. Mater., 41 (1993), pp. 3363-80.

29. C. D. Beachem, Met. Trans. 3 (1972), pp. 437-451.

30. T. Tabata and H. K. Birnbaum, Scripta Metall. 17 (1983), pp. 947-950.

31. I. M. Robertson and H. K. Birnbaum, Acta Metall. 34 (1986), pp. 353-366.

32. H. Matsui, A. Kimura, and H. Kimura: in Strength of Metals and Alloys, P. Haasen, V. Gerold and G. Kostorz, eds., vol. 2, MP 977-87, Pergamon, Oxford, 1979.

33. R. Garber, I. M. Bernstein, and A. W. Thompson, Metall. Trans. A, 12A (1981), pp. 225-34.

34. H. Cialone and R. J. Asaro, Metall. Trans. A, 10A (1979), pp. 376-75.

35. R. A. Oriani and P. H. Josephic, Acta Metall. 22 (1974), pp. 1065-1074.

36. J. W. Hutchinson and V. Tvergaard, Int. J. Mech. Sci., 22 (1980), pp. 339-54.

37. J. W. Hutchinson and V. Tvergaard, Int. J. Solids Structures, 17 (1981), pp. 451-70.

38. L. Anand and W. A. Spitzig, J. Mech. Phys. Solids, 28 (1980), pp. 113-28.